Vol. 42, No. 1 (2020) 131-145, DOI: 10.24874/ti.2020.42.01.13

Tribology in Industry

www.tribology.rs

RESEARCH

Numerical Study on the Influence of the Coating in the Fretting Contact

S. Spinu[a,*]

[a] *Department of Mechanics and Technologies, Stefan cel Mare University of Suceava, 13th University Street, 720229, Suceava, Romania.*

Keywords:

Fretting contact
Numerical simulation
Coatings
Fast Fourier transform
Convolution
Loading path

* Corresponding author:

Sergiu Spinu
E-mail: sergiu.spinu@fim.usv.ro

Received: 9 September 2019
Revised: 1 November 2019
Accepted: 12 December 2019

A B S T R A C T

An existing algorithm for the fretting contact of homogeneous materials is enhanced by incorporating a novel technique for rapid calculation of stresses and displacements in the coated body. State-of-the-art methods for computation of convolution products in the Fourier transform domain allow for fine spatial discretization and accurate reproduction of the loading history. The algorithm is structured on three levels of iterations, and the acceleration of the convolution calculation in the innermost level promises well converged solutions. The frequency response functions derived in the literature are used for the conversion of the required influence coefficients, allowing computation of the half-space response to prescribed loading. The computer program is first validated against the analytical solution for the fretting loop of homogeneous and similarly elastic materials. The refined method is then employed to study the influence of the elastic moduli ratio between the coating and the substrate, on the contact tractions and stresses in the stabilized fretting contact. The presented simulation scenarios prove the method ability to advance the understanding of the transient coated contact.

1. INTRODUCTION

Numerous industrial mechanisms undergo oscillating load conditions, as induced for example by vibration, which result in minute repeated relative surface motion in the mechanical contacts. This fretting condition and its damages, i.e. the fretting wear and the fretting fatigue, degrade the quality of the surface layer by inducing micropits, and decrease the fatigue strength of the contacting components. Although fretting is intrinsically a multidisciplinary process, comprising adhesion, oxidation, abrasion and pitting, a chief role is attributed in the literature to the contact stresses. Derivation of these stresses is especially difficult in the contact of dissimilarly elastic materials, case that requires computationally intensive numerical solutions, such as the finite element method (FEM). A particularly interesting alternative, based on the boundary element method (BEM), capable of elegant and accurate solutions achieved with limited computational resources, was designed

and improved in the literature of contact mechanics, and will be employed and enhanced in this paper as well.

An important breakthrough in the numerical modelling of the contact processes was achieved with the contact solver advanced by Polonsky and Keer [1], and with the technique [2,3] for the calculation of convolution products in the frequency domain. Subsequent iterations allowed for the numerical solution of the fretting contact of homogeneous materials. Gallego et al. [4] modelled the sliding fretting contact by solving repeatedly the contact problem in the normal direction, with consideration of the change in conformity due to wear. A solution for the derivation of tangential tractions in the partial-slip contact was later advanced by Chen and Wang [5]. They predicted the effect of a monotonically increasing tangential force in the point contact between dissimilarly elastic materials, but without reproduction of the loading path. The partial slip contact under a tangential force and a twisting moment was further analyzed by Wang et al. [6]. Method refinement was subsequently achieved by reproduction of the loading path, although the solution convergence was not properly discussed. Gallego, Nélias, and Deyber [7] provided a fully working numerical model for the fretting contact of homogeneous materials, whereas Wang et al. [8] extended the model proposed in [5] to the case of a layered half-space, and Wang et al. [9] applied the latter model to the fretting contact. An alternative approach, capable of simulating the transient frictional contact with slip and stick over a prolonged period of service, was proposed by Spinu and Glovnea [10], and by Spinu and Amarandei [11], whereas Spinu and Frunza [12] studied the hysteretic effects in the fretting contact of dissimilarly elastic materials. Nyqvist et al. [13] recently advanced a new three dimensional model for non-conformal contacts of multilayered rough surfaces subjected to normal and tangential surface loads, but only the gross sliding case was considered.

The static contact of layered materials was studied [8,9,14-16] under different regimes and conditions by making use of the frequency response functions (FRF) describing the response of the layered half-space to load, calculated in the frequency domain. Important research efforts [3,8,14,17] were dedicated to the assessment of the closed form expressions of these FRFs, concluding with the recurrent expressions recently derived by Yu, Wang and Wang [18].

This paper presents new results concerning the contact stresses attained in the fretting contact once a periodic stability is reached. The influence of the coating on the contact tractions and on the subsurface stresses is assessed by computer simulation. The accuracy of the numerical results is guaranteed by the fine spatial meshing of the contact region, and also by the small load increments imposed in the reproduction of the loading path. These well-converged solutions are achieved with a reasonable computational effort due to a newly proposed method of derivation of the required influence coefficients from the FRFs.

2. FRETTING CONTACT MODEL

The fretting contact is best described in the frame of the partial slip contact, in which, although no sliding occurs between the bulks of the contacting bodies, there exist micro-slip at specific points on the contact area. The analytical description of this contact process was independently established by Cattaneo [19] and by Mindlin [20], and relies on the fact that a contact area in full stick does not obey the laws of linear theory of elasticity, as infinite stresses result for the periphery of the contact zones. Consequently, a slip (often referred to as micro-slip) region has to be assumed, which grows from the boundary to the inside of the contact area with the tangential load level, until full slip (i.e., between the bulks of the bodies) occurs at a load level defined by the Amontons' law of friction. Assuming that the tangential load oscillates around zero (i.e., alternates in sign) with an amplitude smaller than the aforementioned limiting load, a model for the fretting contact becomes readily available.

Although contact scenarios with gross slip are employed in experimental investigations of fretting due to the straightforward set up of the testing apparatus, most fretting problems encountered in practice, e.g. bolted or riveted connections or dovetail roots of turbine blades, do not involve gross sliding. The framework of

the frictional contact undergoing partial slip, established in the literature of contact mechanics [21], is thus the starting point in the modelling of the fretting contact processes. The non-conforming point contact is usually considered as reference as it provides conditions that are controllable and repeatable in experimental investigations, and allows for the use of the half-space approximation in the displacement computation. The main model relation is constructed by equating the geometric parameters before and after the elastic deformation caused by the load transmitted through the contact. By reporting the contact problem to a Cartezian coordinate system (x_1, x_2, x_3) with the origin in the initial point of contact and with the x_3-axis pointing inward the coated body (i.e., the normal direction of the contact process), the sum u_i, $i = 1,2,3$, of displacements of the contacting bodies can be expressed in matrix form as:

$$\begin{bmatrix} \Delta u_1 \\ \Delta u_2 \\ u_3 \end{bmatrix} = \begin{bmatrix} \Delta s_1 \\ \Delta s_2 \\ h - h_{\text{init}} \end{bmatrix} + \begin{bmatrix} \Delta \delta_1 \\ \Delta \delta_2 \\ \delta_3 \end{bmatrix}, \qquad (1)$$

where s, δ denote the relative slip distances and the relative displacements between distant points in the two contacting bodies, respectively, in the directions indicated by the subscript, and h_{init} and h the initial (i.e., prior the deformation) and the final gap between the bounding surfaces measured along the normal direction. A schematic of the considered contact model in the plane (x_1, x_3) is depicted in Fig. 1.

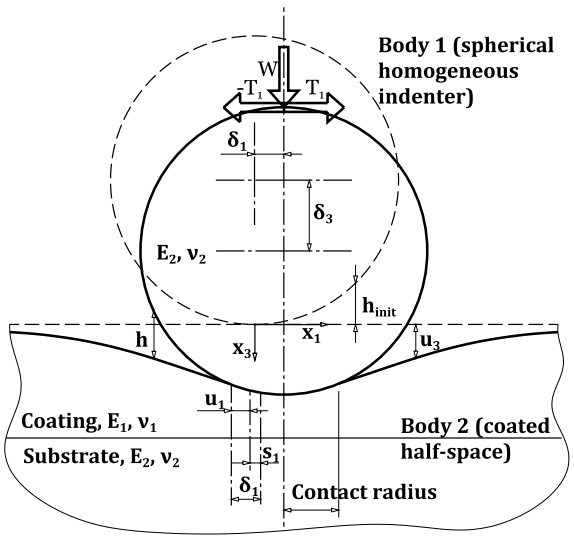

Fig. 1. Fretting contact schematic.

Nonetheless, the contact study performed in this paper addresses the three-dimensional case. While both contacting bodies are considered elastic, the lower body is a coated half-space, whereas the upper body is a homogeneous spherical indenter having the same elastic properties as the substrate of the counter body. The coating is assumed perfectly bonded to the substrate.

The relations for the tangential directions x_1 and x_2 must be considered in incremental form, as suggested by the finite difference symbol Δ in equation (1), accounting for the fact that, unlike the case of the purely normal load when the final state depends on the loading level alone, the tangential contact solution is path-dependent and require the reproduction of the loading history. This hysteretic behaviour, discussed in detail in [11], is also suggested by the presence of friction as a dissipative process.

The analytical solution [19,20] is valid for the contact of similarly elastic materials, and cannot be translated to the case considered in this paper without significant loss of precision. The treatment of the frictional contact of dissimilarly elastic materials requires numerical methods, such as the FEM, the BEM or the semi-analytical methods (SAM). The latter has the advantage of computational efficiency, related primarily to the fact that discretization is needed only in a domain enveloping the contact region, as opposed to FEM which requires the meshing of the bulk. SAM is constructed around the so-called influence coefficients [1], which result from integration of fundamental solutions for stress and displacements induced in a half-space by unit point forces over elementary domains. The influence coefficients provide support for the numerical calculation of displacement and stresses induced by prescribed contact tractions, thus allowing for an iterative search of the unknown regions of interest: the contact area and its slip/stick partition.

In this paper, a rectangular mesh is considered in the common plane of contact, expected to contain the contact area, and the problem parameters are assumed piecewise constant, as thoroughly described in [1]. As contribution of each contact traction q_j, $j = 1,2,3$, to the displacement along the i-axis, $i = 1,2,3$, can be

expressed as a convolution product (denoted by the "$\otimes$" symbol) involving the relevant influence coefficients, the displacement field can be expressed using Einstein summation convention:

$$u_i = u_i^{(2)} - u_i^{(1)} = C_{ij}^{(2)} \otimes q_j^{(2)} - C_{ij}^{(1)} \otimes q_j^{(1)}, \quad (2)$$

where the superscript denotes the referred contacting body. The influence coefficients $C_{ij}^{(k)}$ thus describe the displacement along the direction of $\vec{x}_i$ induced in the body k by the contact traction q_j. Considering that $q_j^{(1)} = -q_j^{(2)}$ for $j = 1,2$, and $q_3^{(1)} = q_3^{(2)}$, as from the definition of contact pressure, a simplified notation will be used in the following relations, by defining the contact tractions $q_j = q_j^{(2)}$, $j = 1,2,3$. Using matrix notation, the displacement field in equation (2) becomes:

$$\mathbf{u} = \mathbf{C} \otimes \mathbf{q}, \text{ where} \quad (3)$$

$$\mathbf{C} = \begin{bmatrix} C_{11}^{(2)} + C_{11}^{(1)} & C_{12}^{(2)} + C_{12}^{(1)} & C_{13}^{(2)} - C_{13}^{(1)} \\ C_{21}^{(2)} + C_{21}^{(1)} & C_{22}^{(2)} + C_{22}^{(1)} & C_{23}^{(2)} - C_{23}^{(1)} \\ C_{31}^{(2)} - C_{31}^{(1)} & C_{32}^{(2)} - C_{32}^{(1)} & C_{33}^{(2)} + C_{33}^{(1)} \end{bmatrix}. \quad (4)$$

The calculation of $C_{ij}^{(1)}$ (i.e., for the homogeneous body) is now classical [1] in the SAM framework and straightforward due to the existence of the closed–form solution to the Boussinesq and Cerruti problems for the homogeneous half-space. The Discrete Convolution Fast Fourier Transform (DCFFT) algorithm [2] presents itself as a state-of-the art technique providing both efficient and precise calculation of the convolution products. The continuous linear convolution in equation (2) is converted into a discrete cyclic convolution by means of the DCFFT, and the convolution calculation is carried out on a virtual domain just two times the initial domain in each physical (in our case, tangential) direction. It is asserted [2] that the DCFFT technique brings no additional error (i.e., no periodicity error) other than the discretization error.

However, the treatment of the coated half-space and of the $C_{ij}^{(2)}$ involves a more elaborate procedure, as the counterparts of the Boussinesq and Cerruti problems for the coated half-space have closed-form solutions only in the frequency domain. A procedure for the derivation of the elastic response (i.e., stresses and displacements) of the coated half-space from the latter solutions (also referred to as the frequency response functions) was previously derived by Spinu [22], involving calculations in the frequency domain on an extended virtual domain to avoid the periodicity error. In this paper, an alternate technique is proposed, aiming to obtain the influence coefficients in the space domain from the FRF, thus allowing the use of the DCFFT technique for coated body as for the homogeneous one. The details of this more computationally effective implementation are given in the next section.

Once the calculation of the displacement field can be achieved for prescribed distributions of surface tractions, the solution of the transient contact problem can be pursued. The latter solution was previously obtained [10] for the fretting contact of homogeneous bodies, but translates well to the case of heterogeneous materials. Basically, the set of equations (1) is divided into two set of equations, one for the normal and the other for the tangential contact direction. By plugging equation (2) into relation (1), one can obtain for the normal direction:

$$C_{31} \otimes q_1 + C_{32} \otimes q_2 + C_{33} \otimes p = h - h_{\text{init}} + \delta_3. \quad (5)$$

The solution in p of the latter equation can be achieved for prescribed yet arbitrary shear tractions q_1 and q_2 by using the algorithm proposed by Polonsky and Keer [1]. This algorithm involves an iterative search of the contact area and of the pressure distribution, which must satisfy simultaneously equation (5), the static force equilibrium:

$$\iint p dx_1 dx_2 = W, \quad (6)$$

as well as the boundary conditions, requiring that, on the contact region, $p > 0$ and $h = 0$, as opposed to the non-contact parts of the computational domain, where $p = 0$ and $h > 0$. The conjugate gradient method is employed to solve efficiently the linear system of equations resulting from the digitized counterpart of equation (5), with nodal pressures as unknowns.

The contact process in the tangential direction is described by the incremental equation:

$$\begin{bmatrix} C_{11} & C_{12} & C_{13} \\ C_{21} & C_{22} & C_{23} \end{bmatrix} \otimes \begin{bmatrix} \Delta q_1 \\ \Delta q_2 \\ \Delta p \end{bmatrix} = \begin{bmatrix} \Delta s_1 + \Delta \delta_1 \\ \Delta s_2 + \Delta \delta_2 \end{bmatrix}, \quad (7)$$

from which a linear system having the increments of the shear tractions as unknowns, can be formed under the assumption of known, yet arbitrary, pressure distribution. The solution of the latter system can be obtained through an algorithm with the same structure as the one for the normal direction, as detailed in [10]. To achieve a unique solution, the static force equilibrium:

$$\iint q_1 dx_1 dx_2 = T_1, \quad \iint q_2 dx_1 dx_2 = T_2, \quad (8)$$

as well as the boundary conditions, differentiating between the slip and the stick regions, should be added. In the slip regions, a new load increment yields relative displacement between initially matching points on the contacting surfaces, so that $(\Delta s_1)^2 + (\Delta s_2)^2 > 0$, and the shear stresses obey a kinetic type law of friction: $\sqrt{q_1^2 + q_2^2} = \mu p$. Here, μ is the coefficient of friction, assumed uniform on the contact area and constant during the loading history. However, this assumption is not a model limitation, as a mapped (in both time and space) distribution of μ can also be considered. In the stick regions, on the other hand, the displacements related to the new load increment are the same on both contacting bodies, i.e. $(\Delta s_1)^2 + (\Delta s_2)^2 = 0$, and stresses follow a static frictional regime: $\sqrt{q_1^2 + q_2^2} < \mu p$.

In should be noted that the static equilibrium equations (6) and (8) tacitly assume that there exist no bending or torsional moments. A bending moment M_1 or M_2 could only be transmitted through a surface (i.e., conformal) contact, whereas the case considered in this paper is concentrated. The torsional moment M_3 is also neglected for brevity, meaning only the fretting modes I (transversal slips) and II (radial slips) are considered, while the fretting mode III (circumferential slips) is not accounted for. However, a complete contact solver comprising the complete force and moment static equilibrium was developed in a previous work [11].

In other words, contact pressure and contact area can be calculated if the shear tractions are known, yet arbitrary, and vice versa, the shear tractions can be assessed for known, yet arbitrary, pressure. This is a first inner level of iterations in the solution of the fretting contact problem. An outer level can be designed [10,11] to stabilize the contact processes in the normal and in the tangential directions, thus accounting for the interdependence between the two set of equations. It involves solving successively the normal and the tangential systems of equations until one major parameter (e.g., contact pressure), does not vary significantly from one iteration to the next. This is the second (intermediate) level of iterations, which is charged with finding the contact solution for a specific load level. The third and outer level of iteration reproduces the loading history by application of the load in increments small enough to assure solution convergence. Adding the time parameter in the contact model may be misleading, because the contact parameters or the material properties does not depend on time, as in the case of viscoelastic materials, and the speed at which the load is applied is of no consequence, as the contact is considered quasi-static. The algorithm flow-chart outlining the intermediate and the outer levels of iterations is presented in Fig. 2, whereas the inner loop is depicted in Fig. 3. A detailed description of the algorithm steps, allowing for efficient implementation in a programming language, can be found in [11]. The algorithm can also be used for gross slip, in which case the shear tractions are simply calculated as the product between pressure and the frictional coefficient. With this simplification, the intermediate loop is eliminated, being replaced by a single instance of the inner loop employed to obtain the contact pressure.

Moreover, when the contacting materials have similar elastic properties, the outer level of iterations is only necessary if the tangential load changes monotony. More precisely, for similarly elastic materials, each change in the sign of the tangential load increment requires exactly one load increment. The contact of materials with different elastic parameters however requires a very fine temporal mesh to avoid jagged stresses profiles. This translates in a significant computational burden related to the calculation of the convolution products in equation (2).

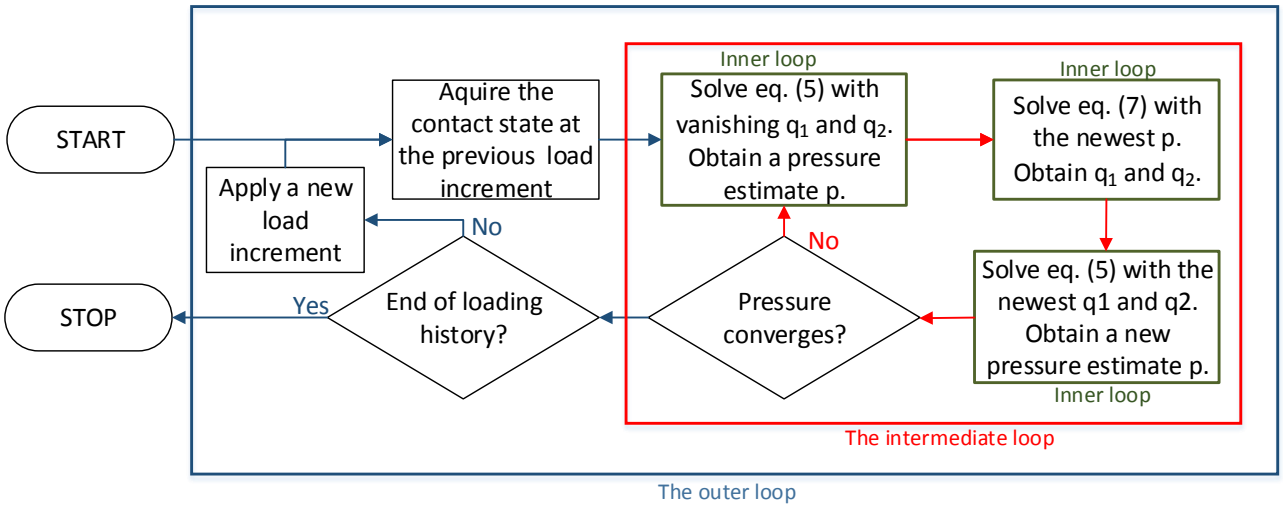

Fig. 2. The flow-chart of the outer and the intermediate loops, including three instances of the inner loop.

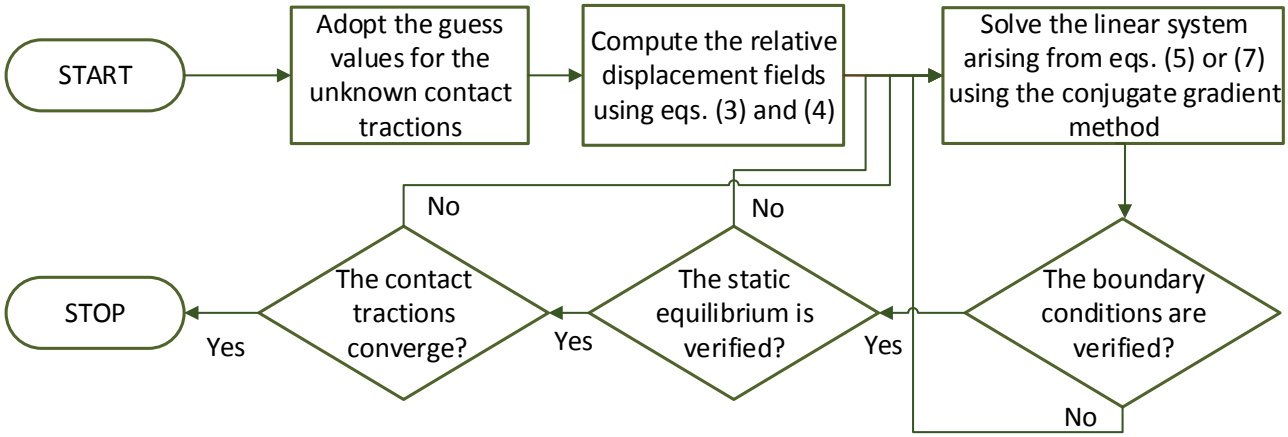

Fig. 3. The flow-chart of the inner loop.

As the derivation of both pressure distribution and shear stresses is achieved in an iterative manner, the displacement calculation has to be performed on each iteration of the inner loop. If N_1, N_2 and N_3 denote the number of iteration of the inner, the intermediate and the outer level of iterations, respectively, then the number of convolutions to be computed for a contact simulation is $2N_1N_2N_3$. Increasing the computational efficiency of the convolution calculation is of paramount importance to allow fine spatial meshes and/or an accurate reproduction of the loading history. The DCFFT technique is currently state-of-the-art for discrete cyclic convolution calculation, but cannot be applied directly to layered materials, because the analytic relation (i.e., the Green's function for the layered material) needed for the calculation of the influence coefficients in the space domain, is missing. A method of derivation of the required influence coefficients from the FRFs (i.e., counterparts of the Green's functions in the frequency domain) is explored in the next section.

3. ACCELERATION OF COMPUTATION

The source of the computational efficiency of the DCFFT stems from the calculation of the convolution in the frequency domain, where the mathematical operation of convolution, of order $O(N^2)$ for series with N members, is converted into an element-wise product of order $O(N)$, according to the convolution theorem. The downside consists in the need for transfer to and from the frequency domain, which can be accomplished by the fast Fourier transform (FFT) in $O(N \log N)$ operations, and more importantly, the implicit problem periodization that contaminates the result. Practically, when no additional treatment is performed, the

calculated output is not only due to the considered non-periodical input, but to an infinitely extended periodical input having the discretization window as period. The DCFFT allegedly avoids completely this periodicity error by performing the calculations on a virtual domain twice (in every physical direction) the problem domain.

In case of problems with known frequency response functions but unknown Green's functions, the calculation can be performed directly in the frequency domain, as suggested in [15], but the required extension of the problem domain is much larger [16] and introduces a heavy computational burden. Considering that the bulk of the computational resources in the fretting contact solution is spent on convolution calculations, reducing that load is of utmost importance. A method of obtaining the influence coefficients needed in the DCFFT algorithm, from the frequency response functions, is proposed in this paper. The advantages of this approach consist in: (1) the DCFFT code can be used for the calculation of displacement in the coated body as well, and (2) the number of transfers to and from the frequency domain, calculated on an enlarged domain, is reduced from 2 to 1. Practically, only the derivation of the influence coefficients requires calculations in the inflated domain, and the remaining computations are performed on a domain just double (in every direction) the original one, as demanded by the DCFFT.

The complete description of the newly proposed conversion technique is given as algorithm steps in the following part. For simplicity and clarity, the relations are presented for one dimension only, but extension to multi-dimensional cases is forthright. Let us assume a problem physical domain of length L meshed into N elementary domains on which the problem parameters are assumed piecewise constant. The domain extension should be performed with at least preservation of the data interval $\Delta = L/N$ to keep the aliasing under control, so that the virtual computational domain is described by parameters λL and λN, where λ should be chosen in the interval $(1\cdots12)$ depending on the required precision (higher values lead to more precise results). This meshing in the spatial domain translates in the frequency domain to a domain of length $2\pi/\Delta$ and a grid step $2\pi/(\lambda L)$.

It should be noted that both domains in the space and in the frequency domain are centered on origin (i.e., zero Cartesian coordinate and zero frequency, respectively). Moreover, it is reasonable to choose both γ and N as powers of 2, as the FFT algorithm is performed by zero-padding to the next power of 2. The FRF for the needed output $\tilde{f}$ is then calculated at the established grid points in the frequency domain, resulting in a discrete complex series $\hat{f}$:

$$\hat{f}_i = \tilde{f}(\omega_i), \text{ where} \tag{9}$$

$$\omega_i = 2\pi(i-\lambda N/2)/(\lambda L), i = 1\cdots\lambda N. \tag{10}$$

The direct evaluation of the term $\hat{f}_{\lambda N/2}$ at zero frequency may be impeded by the fact that most FRFs are singular in origin. A circumventing solution was suggested by Nogi and Kato [15], who replaced the missing sample by the numerically evaluated average on the elementary cell centered in origin:

$$\hat{f}_{\lambda N/2} = \frac{\lambda L}{2\pi}\int_{-\pi/(\lambda L)}^{\pi/(\lambda L)} \tilde{f}(\tau)d\tau. \tag{11}$$

The terms of the series $\hat{f}$ are then rearranged by translating the ones corresponding to negative frequency (i.e., for $\omega_i < 0$) after those calculated for positive frequency. A new series $\hat{g}_i$, $i = 1\cdots\lambda N$, is thus created, so that:

$$\begin{cases} \hat{g}_i = \hat{f}_{i-1+\lambda N/2}, & i = 1\cdots\lambda N/2+1; \\ \hat{g}_i = \hat{f}_{i-1-\lambda N/2}, & i = \lambda N/2+2\cdots\lambda N. \end{cases} \tag{12}$$

Inverse FFT is then applied to the latter series, resulting in a series g_i, $i = 1\cdots\lambda N$, in the spatial domain, from which the influence coefficients C_i, $i = 1\cdots2N$ needed in the DCFFT algorithm are extracted an positioned so that:

$$\begin{cases} C_i = g_i, & i = 1\cdots N; \\ C_i = 0, & i = N+1; \\ C_i = g_{i+(\lambda-2)N}, & i = N+2\cdots2N. \end{cases} \tag{13}$$

The above series C_i is exactly the series of influence coefficients (with zero-padding and rearranged in wrap-around order) needed in the DCFFT algorithm, which accomplishes the convolution calculation devoid of any periodicity error.

The two-dimensional FRFs needed for the calculation of the influence coefficients $C_{ij}^{(2)}$, $i,j=1,2,3$, were expressed in closed-form in the literature by taking the double Fourier transform of the appropriate Papkovich-Neuber potentials, and by imposing the boundary conditions and the continuity conditions at the layers interface. On the surface (i.e., at $x_3=0$), the normal and tangential tractions must obey the boundary conditions corresponding to a frictional contact problem:

$$\sigma_{33}^{(1)}(x_1,x_2,0)=-p(x_1,x_2), \quad (14)$$

$$\sigma_{3i}^{(1)}(x_1,x_2,0)=-q_i(x_1,x_2),\ i=1,2, \quad (15)$$

whereas the continuity condition of tractions and displacements at the interface yields:

$$\sigma_{3i}^{(1)}(x_1,x_2,h_c)=\sigma_{3i}^{(2)}(x_1,x_2,h_c),\ i=1,2,3, \quad (16)$$

$$u_i^{(1)}(x_1,x_2,h_c)=u_i^{(2)}(x_1,x_2,h_c),\ i=1,2,3. \quad (17)$$

Additional constraints yield from the condition that, at infinity in the half-space (i.e., for large x_3), the solution must remain bounded:

$$u_i^{(2)}(x_1,x_2,\infty)=0,\ i=1,2,3, \quad (18)$$

$$\sigma_{ij}^{(2)}(x_1,x_2,\infty)=0,\ i,j=1,2,3. \quad (19)$$

In equations (14)-(19), superscripts (1) and (2) refer to the coating and the substrate, respectively, whereas h_c denotes the coating thickness. The explicit expressions given in [3], obtained without any partial derivatives existing in other formulations [9], were found more easy to implement in the present numerical approach. The conversion procedure reduces the computational burden and the memory requirements by performing the convolution on series with just $2N$ members instead of λN, with λ going as high as 12 [8]. The derivation of the influence coefficients with the procedure described above still requires application of inverse FFT to a series of λN members. However, this calculation should be executed one time only, because the influence coefficients depend on the distances between the grid points and on the elastic properties of the material, and both of which do not change during the contact process. On the contrary, the other convolution member (i.e., the contact tractions) changes from one iteration to the next, and therefore it is convenient to limit the size of the domain on which the FFT of these tractions is calculated. Thus, with the above technique, the computational cost per iteration is thus reduced to FFTs of series of $2N$ members instead of λN. The savings become important as the numbers of iteration increases, as in the case of the fretting contact. The contact simulations described in the following sections proved that the improved method provided a reduction of 34% in the program execution time compared to the existing method [15]. This reduction is expected to become more significant with longer loading histories.

4. RESULTS AND DISCUSSIONS

A spherical homogeneous indenter of radius $R=0.018$ m, with the Young modulus $E_2=210$ GPa and the Poisson's ratio $\nu_2=0.3$, is loaded against a coated half-space following the loading path depicted in Fig. 2. The elastic parameters of the coating are denoted by E_1, ν_1, whereas the substrate is assumed similarly elastic with the indenter. In the following simulations, E_2, ν_2 and $\nu_1=\nu_2$ are kept constant, whereas the elastic moduli ratio E_1/E_2 is varied. A normal load $W_{max}=1$ kN is first applied, and subsequently an oscillating tangential force is added while keeping the normal load constant. Without losing generality, the tangential force is assumed in the direction of $\vec{x}_1$, and its amplitude is $T_{1max}=0.9\mu W$.

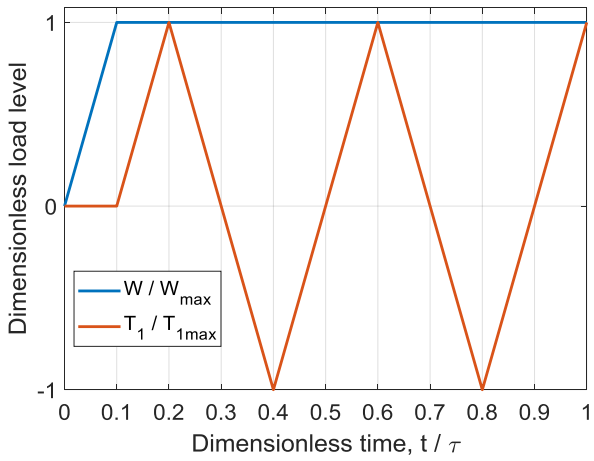

Fig. 4. The loading path.

As depicted in Fig. 4, the simulation reproduces the first three loading trajectories.

It should be noted that in Fig. 4, the time axis features a sequence of discrete times normalized by the length of the simulation window τ, and the absolute magnitude of the time intervals is of no consequence as the contact is assumed quasi-static. Although in the loading window $(0\cdots0.1)\tau$ no tangential force is applied, the contact state at $t=0.1\tau$ cannot be accurately predicted from a pure normal contact model.

Due to the dissimilarity in the elastic properties of the contacting materials, initially matching points on the contact surface undergo different tangential displacements, leading to a tendency to slip that will be resisted by friction. This gives birth to self-equilibrating shear stresses that in their turn affect the pressure distribution. Consequently, the contact state $t=0.1\tau$ requires reproduction of the loading path and load incrementation, backed by the consideration of the tangential effects. A comparison of the pressure and shear stress profiles in the plane $x_2=0$, obtained with and without reproduction of the loading history, is shown in Fig. 5.

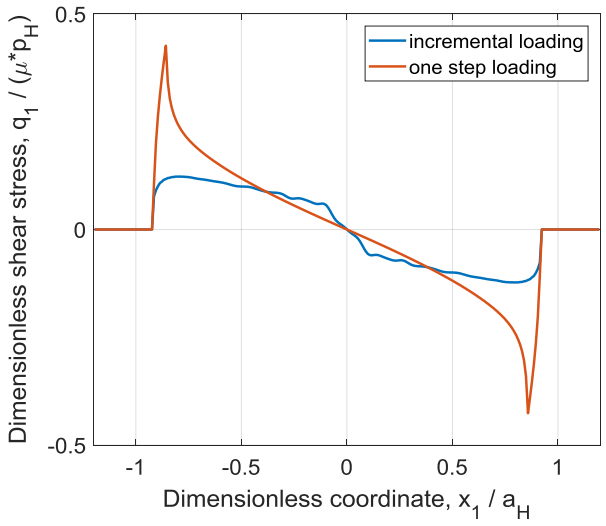

Fig. 5. Dimensionless shear stresses at $t=0.1\tau$, $E_1/E_2=2$.

The newly advanced program for the simulation of the fretting contact involving coatings was benchmarked against the analytical solution [21] for a fretting loop in the contact between similarly elastic materials. To this end, the case $E_1/E_2=1$ was simulated. Whereas the influence coefficients for the upper body $\mathbf{C}^{(1)}$ were calculated from integration of the Boussinesq and Cerruti fundamental solutions for the homogeneous half-space, the conversion technique advanced in this paper was implemented in the $\mathbf{C}^{(2)}$ computation. A perfect equality $\mathbf{C}^{(1)}\equiv\mathbf{C}^{(2)}$ would lead to vanishing shear stresses at time $t=0.1\tau$. The stress depicted in figure 6 is very close to that, although some numerical oscillations exist. This is to be expected giving the complexity of the involved mathematical model.

The frequency response functions given in the literature [3] were implemented in the $\mathbf{C}^{(2)}$ conversion. The stress profiles at subsequent times follow the analytical solution (depicted using grey lines) with no evident deviations. This good validation gives confidence in the capability of the numerical tool to accurately reproduce and predict the investigated fretting contact process.

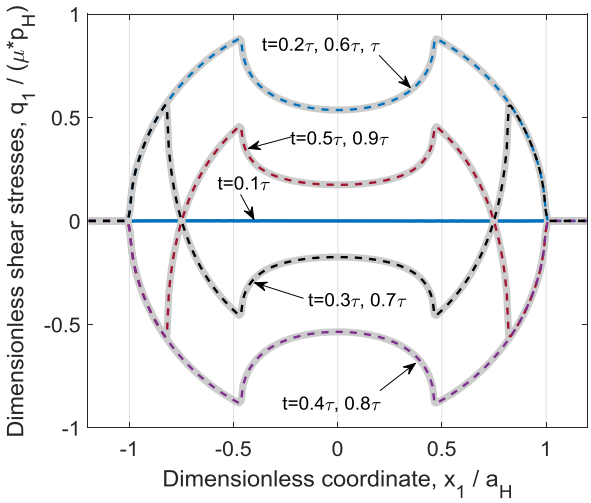

Fig. 6. Dimensionless shear stresses in the fretting contact of similarly elastic bodies.

The influence of the coating on the contact stresses is assessed by varying the elastic moduli ratio between the coating and the substrate. The shear stress profiles in the coated half-space, predicted for various load levels and elastic moduli ratios between the coating and the substrate, are depicted in figure 7. The Hertz contact for the case $E_1/E_2=1$ is taken as reference and its parameters, namely the contact radius a_H and the central pressure p_H, are used as normalizers.

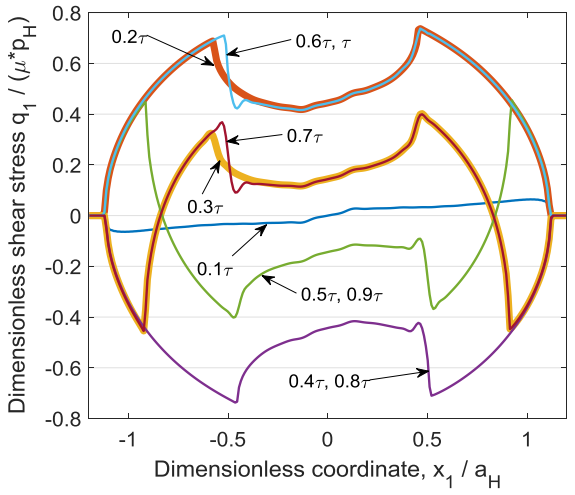

a)

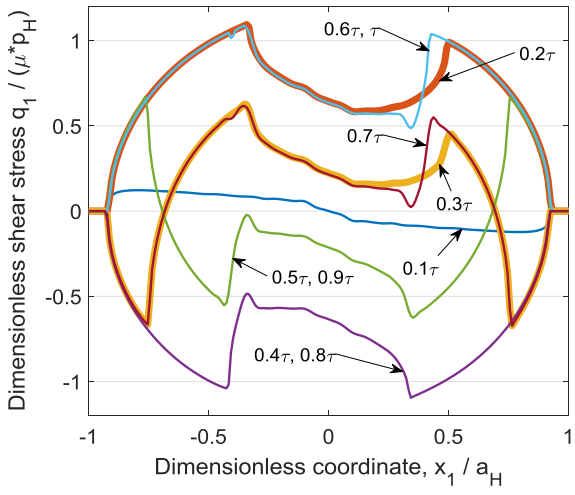

b)

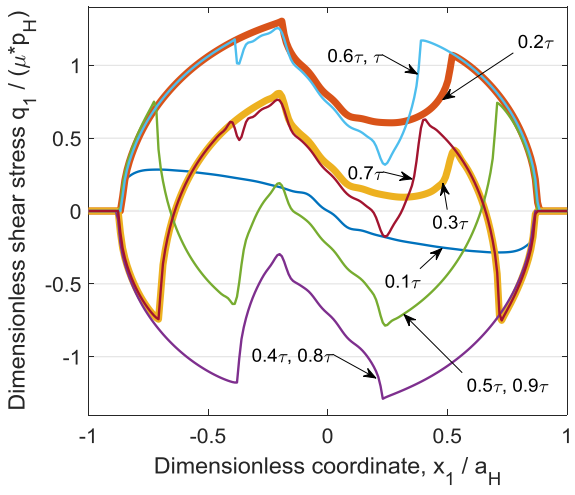

c)

Fig. 7. Dimensionless shear stresses $q_1/(\mu p_H)$ in the plane $x_2=0$: (a) $E_1/E_2=0.5$; (b) $E_1/E_2=2$; (c) $E_1/E_2=4$.

These results were obtained on a 256×256 grid established in a rectangular domain of side lengths $2.4a_H\times2.4a_H$, centered on the initial point of contact. The process path depicted in Fig. 4 was reproduced by imposing $N_3=1000$ load increments, from which the first 100 were reserved for the time period $(0\cdots0.1)\tau$. The averages values for the inner and the intermediate loops were $N_2=7$ and $N_1=20$. A contact simulation for a fixed elastic moduli ratio E_1/E_2 was completed on a quad-core 3.2GHz CPU in less than 3 hours. The frictional coefficient was fixed at $\mu=0.3$, and the coating thickness at a_H.

The simulations suggest that a periodic stability is achieved after the first loading cycles, as shown by the coincidence of the stress curves predicted for $t=0.8\tau$, $t=0.9\tau$ and $t=\tau$, with those for $t=0.4\tau$, $t=0.5\tau$ and $t=0.6\tau$, respectively. Practically, only the first loading-unloading (i.e., from $t=0$ to $t=0.4\tau$) generates truly unique profiles. The stick area is slightly moved opposite to $\vec{x}_1$ for $E_1/E_2<1$ and in the direction of $\vec{x}_1$ for $E_1/E_2>1$. The stress state attained when the tangential force reaches its maximum value, $T_1=T_{1\max}$, is generally a reversal (i.e., with respect to both in-plane axes) of that achieved for the $T_1=-T_{1\max}$.

The shear stresses for $t=0.1\tau$ are self-equilibrating in any radial direction, as suggested by the streamlines of the shear vectors $\mathbf{q}=(q_1,q_2)$ presented in Fig. 8. The shear vectors point to the outside on the more compliant body and to the inside on the stiffer counter body. This is consistent with the general contact theory stating that the direction of the shear tractions opposes relative motion of the surfaces, i.e.:

$$\operatorname{sgn}(\mathbf{q})=-\operatorname{sgn}(\partial\mathbf{u}/\partial t), \tag{20}$$

where the time-derivative of the relative displacement $\mathbf{u}=\mathbf{u}^{(2)}-\mathbf{u}^{(1)}$, with upper indexes denoting the two contacting bodies, should be considered as finite differences between discrete values corresponding to the time moments in which the loading history is replicated.

The streamlines of the shear vectors for the last simulated increase of the tangential load (i.e., from $t=0.8\tau$ to $t=\tau$) are depicted in Fig. 9 for the case $E_1/E_2=0.5$ and in Fig. 10 for $E_1/E_2=2$.

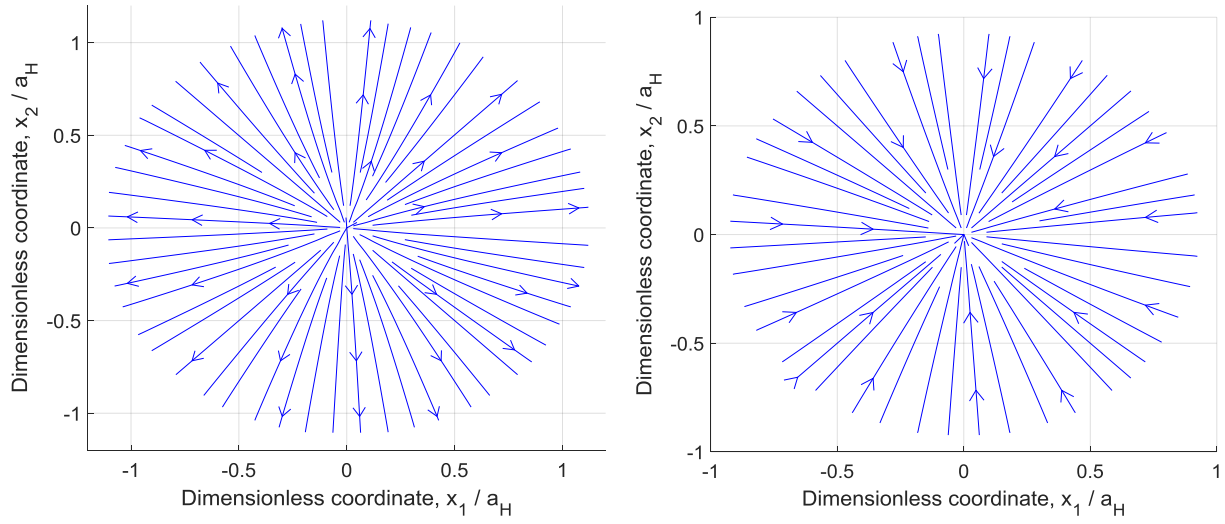

Fig. 8. Streamlines of the shear vectors $\mathbf{q}=(q_1,q_2)$ at: (a) $E_1/E_2=0.5$; (b) $E_1/E_2=2$.

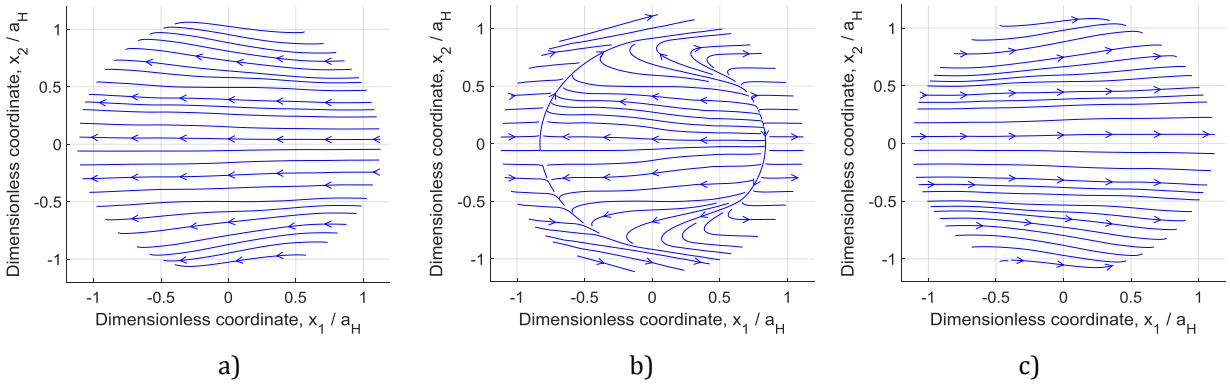

Fig. 9. Streamlines of the shear vectors $\mathbf{q}=(q_1,q_2)$, $E_1/E_2=0.5$: (a) $t=0.8\tau$; (b) $t=0.9\tau$; (c) $t=\tau$.

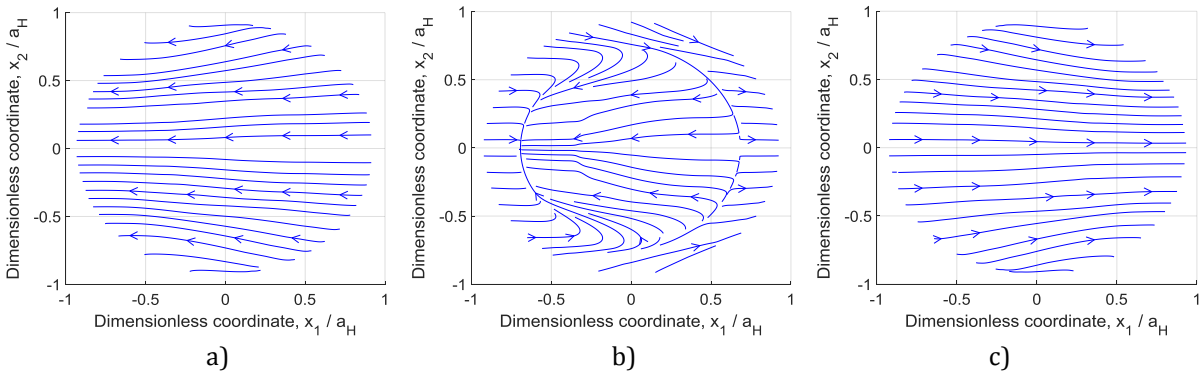

Fig. 10. Streamlines of the shear vectors $\mathbf{q}=(q_1,q_2)$, $E_1/E_2=2$: (a) $t=0.8\tau$; (b) $t=0.9\tau$; (c) $t=\tau$.

A typical stick ratio defined as the ratio between the stick and the (instantaneous) contact area is depicted in Fig. 11. The curves for various elastic moduli ratios are similar, and prove that, when the tangential force increment changes its sign, instantaneous stick sets in, immediately followed by reverse slip at the edge of the contact area. The latter slip covers gradually previous slip regions of the opposite sign, resulting in oscillating slip on specific regions of the contact area. The plot also show that there also exists frictional slip during the normal indentation (i.e., prior to $t=0.1\tau$). Small normal load increments in the beginning of the loading curve are essential to solution convergence.

The tangential displacement of one body relative to the other is plotted in Fig. 12 as a function of

the applied tangential force, forming a complete hysteresis loop, whose area accounts for the work done by the tangential force during a complete cycle. The latter work is dissipated by frictional micro-slip, and repeated load oscillation will generate wear in the annulus of oscillating slip, producing, often in the presence of corrosion, the specific surface damage known as "fretting". The latter is hold responsible for the premature failure of machine elements by fatigue, especially when the components also carry high steady stress.

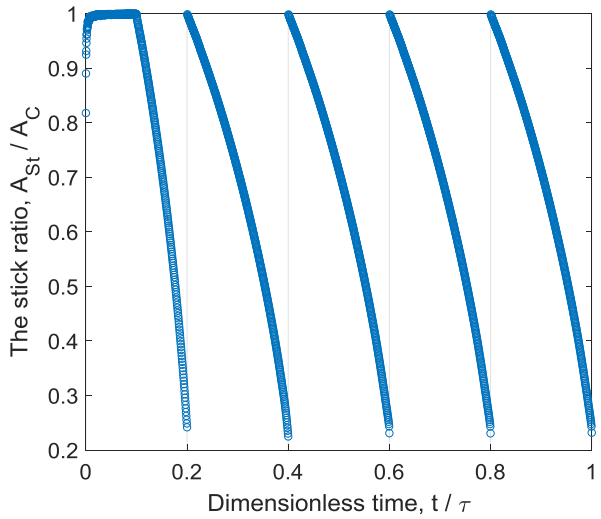

Fig. 11. The stick ratio.

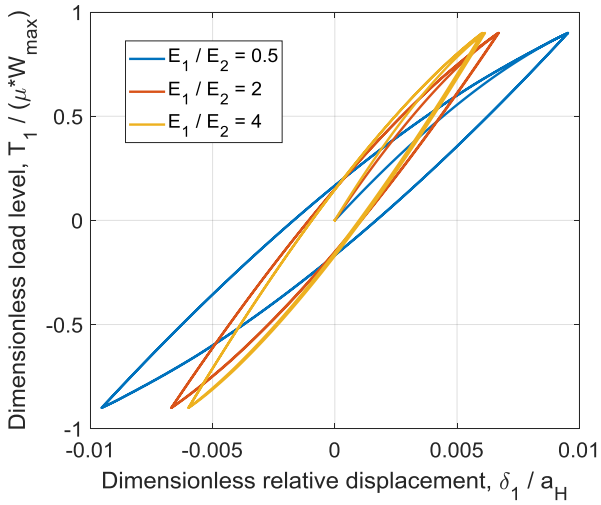

Fig. 12. Load-displacement cycles.

Although not apparent due to the very good superposition, two complete hysteresis loops are depicted in figure 12: the first one for the time period $t \in (0.2\tau;0.6\tau]$, and the second one for $t \in (0.6\tau;\tau]$. At every pass of the tangential force through its extreme values $T_1/(\mu W_{\max}) = \pm 0.9$, i.e. at specific times $t = 0.2t, 0.4t, 0.6t, 0.8t$, instantaneous full stick occurs, as shown in Fig. 11 where the stick ratio A_{St}/A_C approaches unity. The unique branch starting from origin in Fig. 12 corresponds to the time period $t \in (0.1\tau;0.2\tau]$. Although the hysteresis curves for the first two fretting loops are very similar, there exist dissimilarities in the tractions profiles predicted for corresponding points from the two loops, as shown in Fig. 7. The extended loading history in Fig. 4 was considered to confirm a stabilized periodicity in both the hysteresis loops and the tractions profiles after the first loading cycles.

Knowledge of the contact tractions indicates the oscillating slip region were the attrition of the contact interface is expected to occur, but also allows calculation of the subsurface stresses, in the same manner as the displacements. In the following examples, the stress calculation is performed in 256 layers parallel to the free surface, covering a depth of $2a_H$. The iso-contours of the von Mises equivalent tension, which is a measure of the plastic yield propensity in the elastic contact, corresponding to the end of the simulated loading window, i.e. $t = \tau$, are depicted in Fig. 13 for different elastic moduli ratios between the coating and the substrate. Position of the maximum is indicated with the "X" mark and its magnitude is specified on each plot. The numerical results suggest that the maximum stress intensity is located in the more compliant coating, i.e. when $E_1/E_2 = 0.5$, Fig. 11a, whereas increasingly harder coatings place the maximum on the free surface, Fig. 11b, and at the interface between the coating and the substrate, Fig. 11c. The latter position is particularly detrimental because is the source of cracks probable to originate in the thinner coatings [23]. The shift of the stress iso-contours in the direction of $\vec{x}_1$ is a direct result of the distributions of shear tractions depicted in Fig. 7, showing the influence of the elastic mismatch E_1/E_2 on the position of the stick region. As a result of the elastic dissimilarity between the contacting materials and of the coupling between the normal and the tangential effects, the stick zone is moved toward negative x_1 for $E_1/E_2 < 1$ and in the opposite direction for $E_1/E_2 > 1$, which also perturbs the symmetry of the subsurface tractions.

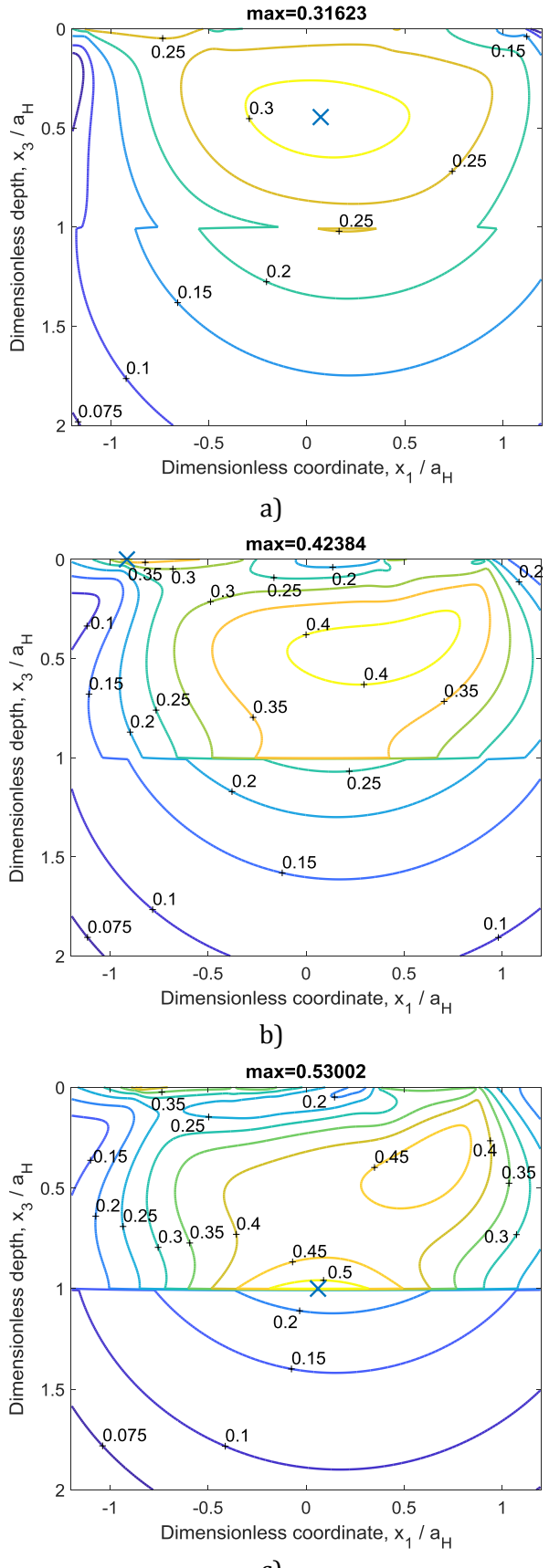

Fig. 13. Iso-contours of the dimensionless von Mises equivalent stress σ_{VM}/p_H in the plane $x_2 = 0$ at $t = \tau$: (a) $E_1/E_2 = 0.5$; (b) $E_1/E_2 = 2$; (b) $E_1/E_2 = 4$.

The established contact model can be further coupled with a wear model that quantify the wear of a sliding contact, e.g. [24,25], resulting in a efficient contact analysis tool capable of predicting the wear volume and the accompanying change of the surface geometry due to wear, as a function of the sliding distance, the applied normal load, the hardness of the softer material and the frictional coefficient. However, more complex mechanisms such as the creation and the ejection of debris that modify the frictional coefficient, should be considered for realistic contact simulations.

5. CONCLUSIONS

The performance and service life of the mechanical coated contact subjected to fretting relies on the accurate prediction of the slip regions and the stress state in the contacting bodies. These chief goals are achieved in this paper by numerical simulation assisted by the fast Fourier transform.

A contact solver originally proposed for homogenous but dissimilarly elastic bodies is enhanced to the case of layered materials. The huge computational burden related to the stress and displacement calculation in the heterogeneous body is partially relieved by proposing a method of conversion of the influence coefficients from the frequency response functions available in the literature for the bilayered material. In this manner, a state-of-the-art technique for the acceleration of convolution computation, previously applied to homogeneous solids, can be employed to coated bodies. The computational advantage allows the consideration of a well-converged reproduction of the loading path, including the initial normal indentation which is often neglected in the literature. The considered loading window was long enough as to predict the attainment of a periodic stability after the first unique loading branch.

The predictions of the newly proposed computer program compare well with the closed-form solution for the fretting of similarly elastic homogenous bodies. New and accurate distributions of contact tractions and subsurface stresses are presented for various elastic moduli ratios between the coating and

the substrate. The performed numerical simulations prove the method ability to solve the complex problem of fretting in the coated contact with high accuracy, within the limits of a reasonable computational effort.

REFERENCES

[1] I.A. Polonsky, L.M. Keer, *A Numerical Method for Solving Rough Contact Problems Based on the Multi-Level Multi-Summation and Conjugate Gradient Techniques*, Wear, vol. 231, iss. 2, pp. 206-219, 1999, doi: 10.1016/S0043-1648(99)00113-1

[2] S. Liu, Q. Wang, G. Liu, *A Versatile Method of Discrete Convolution and FFT (DC-FFT) for Contact Analyses*, Wear, vol. 243, iss. 1-2, pp. 101-111, 2000, doi: 10.1016/S0043-1648(00)00427-0

[3] S. Liu, Q. Wang, *Studying Contact Stress Fields Caused by Surface Tractions With a Discrete Convolution and Fast Fourier Transform Algorithm*, Journal of Tribology, vol. 124, iss. 1, pp. 36-45, 2001, doi: 10.1115/1.1401017

[4] L. Gallego, D. Nélias, C. Jacq, *A Comprehensive Method to Predict Wear and to Define the Optimum Geometry of Fretting Surfaces*, Journal of Tribology, vol. 128, iss. 3, pp. 476–485, 2006, doi: 10.1115/1.2194917

[5] W.W. Chen, Q.J. Wang, *A Numerical Model for the Point Contact of Dissimilar Materials Considering Tangential Tractions*, Mechanics of Materials, vol. 40, iss. 11, pp. 936-948, 2008, doi: 10.1016/j.mechmat.2008.06.002

[6] Z.-J. Wang, F.-M. Meng, J.-X. Xiao, W.-Z. Wang, *Numerical Analysis of Partial Slip Contact under a Tangential Force and a Twisting Moment*, Proceedings of The Institution of Mechanical Engineers Part J: Journal of Engineering Tribology, vol. 225, iss. 2, pp. 72-83, 2011, doi: 10.1177/2041305X10392125

[7] L. Gallego, D. Nélias, S. Deyber, *A Fast and Efficient Contact Algorithm for Fretting Problems Applied to Fretting Mode I, II and III*, Wear, vol. 268, iss. 1-2, pp. 208-222, 2010, doi: 10.1016/j.wear.2009.07.019

[8] Z.-J. Wang, W.-Z. Wang, H. Wang, D. Zhu, Y.-Z. Hu, *Partial Slip Contact Analysis on Three-Dimensional Elastic Layered Half Space*, Journal of Tribology, vol. 132, iss. 2, p. 12, 2010, doi: 10.1115/1.4001011

[9] Z.J. Wang, W.Z. Wang, F.M. Meng, J.X Wang, *Fretting Contact Analysis on Three-Dimensional Elastic Layered Half Space*, Journal of Tribology, vol. 133, iss. 3, p. 8, 2011, doi: 10.1115/1.4004104

[10] S. Spinu, M. Glovnea, *Numerical Analysis of Fretting Contact between Dissimilarly Elastic Materials*, Journal of the Balkan Tribological Association, vol. 18, iss. 2, pp. 195-206, 2012.

[11] S. Spinu, D. Amarandei, *Numerical Simulation of Slip-Stick Elastic Contact*, in M. Andriychuk (Ed.): Numerical Simulation, IntechOpen, pp. 129-154, 2012, doi: 10.5772/48451

[12] S. Spinu, G. Frunza, *The Hysteretic Behaviour of Partial Slip Elastic Contacts Undergoing a Fretting Loop*, Journal of Physics: Conference Series, vol. 585, p. 8, 2015, doi: 10.1088/1742-6596/585/1/012007

[13] J. Nyqvist, A. Kadiric, S. Ioannides, R. Sayles, *Semi-analytical model for rough multilayered contacts*, Tribology International, vol. 87, pp. 98-112, 2015, doi: 10.1016/j.triboint.2015.01.006

[14] T.C. O'Süllivian, R.B. King, *Sliding Contact Stress-Field due to a Spherical Indenter on a Layered Elastic Half-space*, Journal of Tribology, vol. 110, iss. 2, pp. 235–240, 1988, doi: 10.1115/1.3261591

[15] T. Nogi, T. Kato, *Influence of a Hard Surface Layer on the Limit of Elastic Contact—Part I: Analysis Using a Real Surface Model*, Journal of Tribology, vol. 119, iss. 3, pp. 493–500, 1997, doi: 10.1115/1.2833525

[16] I.A. Polonsky, L.M. Keer, *A Fast and Accurate Method for Numerical Analysis of Elastic Layered Contacts*, Journal of Tribology, vol. 122, iss. 1, pp. 30-35, 1999, doi: 10.1115/1.555323

[17] C. Yu, Z. Wang, G. Liu, L.M. Keer, Q.J. Wang, *Maximum von Mises Stress and Its Location in Trilayer Materials in Contact*, Journal of Tribology, vol. 138, iss. 4, p. 13, 2016, doi: 10.1115/1.4032888

[18] C. Yu, Z. Wang, Q.J. Wang, *Analytical Frequency Response Functions for Contact of Multilayered Materials*, Mechanics of Materials, vol. 76, pp. 102-120, 2014, doi: 10.1016/j.mechmat.2014.06.006

[19] C. Cattaneo, *Sul contatto di due corpi elastici: distribuzione locale degli sforzi*, Accademia Nazionale Lincei, Rendiconti, vol. 27, no. 6, p. 7, 1938. (in Italian)

[20] R.D. Mindlin, *Compliance of Elastic Bodies in Contact*, Journal of Applied Mechanics, vol. 16, iss. 3, pp. 259-268, 1949.

[21] K.L. Johnson, *Contact Mechanics*. Cambridge University Press, Cambridge, 1985, doi: 10.1017/CBO9781139171731

[22] S. Spinu, *Numerical Analysis of Elastic Contact between Coated Bodies*, Advances in Tribology, vol. 2018, p. 13, 2018, doi: 10.1155/2018/6498503

[23] L.M. Keer, C.H. Kuo, *Cracking in a Loaded, Brittle Elastic Half-Space*, International Journal of Solids and Structures, vol. 29, iss. 14-15, pp. 1819–1826, 1992, doi: 10.1016/0020-7683(92)90173-Q

[24] J.F. Archard, *Contact and Rubbing of Flat Surfaces*, Journal of Applied Physics, vol. 24, pp. 981–988, 1953, doi: 10.1063/1.1721448

[25] S. Fouvry, P. Kapsa, L. Vincent, *Quantification of Fretting Damage*, Wear, vol. 200, iss. 1-2, pp. 186–205, 1996, doi: 10.1016/S0043-1648(96)07306-1